Percolation of diffusionally evolved two-phase systems

Victor E. Brunini, Christopher A. Schuh, and W. Craig Carter

Phys. Rev. E **83**, 021119 — Published 28 February 2011

DOI: 10.1103/PhysRevE.83.021119

Percolation of Diffusionally Evolved Two-Phase Systems

Victor E. Brunini, Christopher A. Schuh, and W. Craig Carter*

Department of Materials Science and Engineering,

Massachusetts Institute of Technology, 77 Massachusetts Avenue,

Cambridge, Massachusetts 02139, USA

(Dated: November 22, 2010)

Abstract

Percolation thresholds and critical exponents for universal scaling laws are computed for microstructures that derive from phase-transformation processes in two dimensions. The computed percolation threshold for nucleation and growth processes, $p_c \approx 0.6612$, is similar to those obtained by random placement of disks, and greater than that of spinodal decomposition, $p_c \approx 0.4987$. Three critical exponents for scaling behavior were computed and do not differ significantly from universal values. The time-evolution of a characteristic microstructural length was also computed: for spinodal decomposition, this length grows according to a power law after a short incubation period; for nucleation and growth, there are several transitions in the nature of the growth law. We speculate that the transitions in nucleation and growth derive from competing effects of coalescence at short times and then subsequent coarsening. Short-range order is present, but different, for both classes of microstructural evolution.

PACS numbers: 64.60.ah

*ccarter@mit.edu

I. INTRODUCTION

Percolation theory is of considerable interest for its application to understanding and predicting microstructure-property relationships of multi-phase materials. For two-phase composites, the universal scaling laws of percolation theory can be used to predict linear material properties— diffusivity, conductivity, and elasticity—over a large range of the phase fraction ϕ. By comparison, mean field approaches for composite material behavior can provide rigorous material-property bounds, but are usually accurate only in the dilute limits of ϕ. Thus, mean field approaches are difficult to apply when properties are governed by phase topology and connectivity, whereas percolation theory's scaling laws provide material-property estimates near the percolation threshold. These estimates scale as $|\phi - \phi_c|^b$: a property-dependent power, b, of the deviation of the phase fraction from the percolation threshold ϕ_c. The amplitudes and exponents for various property scaling laws are known and tabulated [1, 2].

Percolation thresholds ϕ_c are known for many different types of arrangements of *random* phases (e.g., square and triangular lattices, non-overlapping disks) [3–10]. However, materials rarely have random phase distributions: correlations are produced during processing or microstructural evolution. Finite-range correlations in the phase distribution do not change the universal scaling relations, however they do shift the percolation threshold, p_c, from its known value in the random case [3, 11–23]. Scaling law estimates depend on shifts of p_c produced by such correlations, but in general these shifts are poorly understood in a quantitative sense. While universal scaling relations are powerful predictors of material properties, they cannot be applied when the percolation threshold is unknown—and it is unknown for the majority of observed microstructures, which are correlated.

Correlations and the shift they induce in the percolation thresholds have been studied in many specific systems [16–18, 22, 24–39]. In most of these studies, correlations are induced artificially, or are intended to simulate some known effects of processing, as in the case of composite materials that are formed by mixing phases [27, 32, 34, 40, 41]. However, one important class of materials has received relatively little attention: microstructures that form by a process of phase separation. Some prior work has examined the growth of clusters during nucleation and growth and spinodal decomposition in Ising models, but we are not aware of any work in the phase transformation literature that methodically studies the

percolation transition [42–44]. In engineering contexts, most multi-phase microstructures derive from phase transformations (e.g., eutectic, eutectoid or spinodal decomposition, or by the nucleation and growth of a second phase in a matrix of the first). In these cases, the resulting phase distribution is correlated. Decomposition processes involve local diffusional fields that produce patterns in the resulting phases, such as the lamellar structure characteristic of eutectic or eutectoid decomposition, or the bicontinuous spinodal structure. In nucleation and growth transformations, second phase particles interact first through soft impingement of their respective diffusion fields, and later through hard impingement on solid contact; these interactions affect growth and coarsening kinetics and produce spatial phase-distribution correlations.

Although the role of diffusional phase evolution during such transformations is known to affect the resulting structure, we are not aware of any work relating such processes of structural evolution to a shift in the percolation threshold. It is the purpose of this paper to provide the first steps towards addressing this issue: we simulate microstructural evolution from spinodal decomposition and from nucleation and growth processes, and then compute the influence of these different transformation types on spatial correlations and the percolation threshold.

II. SIMULATION METHODS

We use phase-field simulations to study the effects of phase correlations introduced during diffusion-controlled microstructural evolution. Two specific microstructural evolution pathways are considered: (i) spinodal decomposition, and (ii) nucleation and growth. For spinodal decomposition we use a dual well free energy function of the form:

$$F(c) = \frac{16F_{max}}{(c^\beta - c^\alpha)^4}[(c - c^\alpha)(c - c^\beta)]^2 \tag{1}$$

where c^α and c^β are the limiting concentrations of the α- and β-phases, c is the concentration of the B-component and F_{max} is the height of the saddle point between the wells [45]. For concentrations within the miscibility gap, $c^\alpha < c < c^\beta$, the equilibrium β-phase fraction, p_∞, is determined by the lever rule: $p_\infty = (c_0 - c^\alpha)/(c^\beta - c^\alpha)$ where c_0 is the system's average concentration [49]. The evolution of $c(\vec{x}, t)$ is simulated with the Cahn-Hilliard equation:

$$\frac{\partial c}{\partial t} = M_c \left[\bigtriangledown^2 \frac{\partial F(c)}{\partial c} - \epsilon_c^2 \bigtriangledown^4 c \right] \tag{2}$$

where M_c is a positive kinetic coefficient, F is the free energy function given in Equation 1 and ϵ_c is the diffuse-interface parameter controlling the energy penalty due to concentration gradients [46]. The numerical values used for all simulation parameters are listed in Table I.

To study the universal scaling parameters dependence on the β-phase fraction for the spinodal case, decomposition is assumed to initiate from a nearly uniform concentration field $c(x, y, t = 0) = c_0 + \delta$ where $c_0 = c^a\alpha + p_\infty(c^\beta - c^\alpha)$ for $0 < p_\infty < 1$ and δ is chosen from a uniform random distribution $-10^{-3} < \delta < 10^{-3}$ at each node on a discrete square grid.

For the nucleation and growth simulations, we employ the homogeneous free energy function for a binary eutectic proposed by Wheeler et al., with a few simplifying assumptions [46]. Specifically, we use the dimensionless, symmetric version of their model and assume that the system is isothermal and solid throughout at all times. This model introduces a second phase field parameter, $\psi(x, y)$, representing the spatial variation in phase. The free energy interpolates between the free energy functions for the pure α and β phases based on the local value of $\psi(x, y)$. The resulting free energy function is:

$$\begin{aligned} F(\tilde{T_0}, c, \psi) = \tilde{f_0} + \frac{\tilde{W_\psi}}{4} g(\psi)\tilde{T_0} I(c) \\ + \tilde{L}(\tilde{T_0} - 1)[h(\psi)c + (1 - h(\psi))(1 - c)] \\ + \tilde{L}(\tau\tilde{T_0})[h(\psi)(1 - c) + (1 - h(\psi))c] \end{aligned} \tag{3}$$

where $\tilde{T_0}$ is the dimensionless temperature, $\tilde{W_\psi}$ the dimensionless energy barrier height, and $\tilde{L}$ the dimensionless latent heat. $h(\psi) = \psi^2(3-2\psi)$ and $g(\psi) = \psi^2(1-\psi)^2$ are interpolating functions and $I(c) = c\ln(c)+(1-c)\ln(1-c)$ is an entropic contribution to the Helmholtz free energy [46]. A more detailed derivation and description of the model is found in Wheeler et al. [46]. As in spinodal decomposition, the evolution of the concentration field during nucleation and growth is simulated with the Cahn-Hilliard equation (i.e., Eq. 2 with $F(c)$ replaced by $F(\tilde{T_0}, c, \psi)$). The evolution of ψ is simulated with the Allen-Cahn equation:

$$\frac{\partial\psi}{\partial t} = -M_\psi \left[\frac{\partial F(\tilde{T_0}, c, \psi)}{\partial\psi} - \epsilon_\psi^2 \bigtriangledown^2 \psi \right] \tag{4}$$

where M_ψ is a positive kinetic coefficient, F is the homogeneous free energy function, and ϵ_ψ is a parameter affecting interface width [47].

Simulations of nucleation and growth begin with the system containing primarily α-phase ($\psi \approx 0$), with randomly placed discs of finite ψ that serve as nuclei for the β-phase ($\psi \approx 1$)

[50]. To specify the equilibrium phase fraction, p_∞, the c_0 is chosen by the lever rule as in spinodal decomposition. However, because the averaged perturbation is positive, the algorithm to specify the initial concentration field must be modified. To accomplish this, a second parameter is introduced, p_0^∞, that determines the initial fraction, p_0, of the system covered by nuclei of the β phase according to $p_0 = p_0^\infty p_\infty$.

The algorithm for initializing the system to meet these criteria is as follows. The number of initial nuclei is determined by the value of p_0:

$$N_{\text{nuclei}} = \frac{p_0 N_x N_y}{s}$$

where N_x and N_y are the numbers of discrete grid points in the x- and y-directions and s is the size of each individual nucleus. All nuclei are initially circles of radius $r_0 = 2\text{dx}$, which is the smallest integral radius for supercritical nuclei. s is determined by counting the number of lattice sites that fall within the nucleus. For all simulations we set $p_0^\infty = 0.1$ so that the system is initially at 10% of its equilibrium volume fraction. The concentration of B-component outside of the nuclei needed to arrive at the desired average concentration, c_0, is calculated:

$$c_{\text{else}} = \frac{N_x N_y c_0 - N_{\text{nuclei}} s c^\beta}{N_x N_y - N_{\text{nuclei}} s}$$

The x- and y-values for centers of nuclei are chosen randomly but overlaps are rejected. The concentration and phase fields of each node within a radius $r = r_0$ of x and y is initialized to $c = c^\beta$ and $\psi = 0.99$; otherwise each node (representing untransformed material) is initialized to to $c(x, y) = c_{else}$ and $\psi(x, y) = 0.01$. This process is repeated until all N_{nuclei} are placed.

We use finite difference methods to integrate the governing equations (i.e., Eq. 2 for spinodal decomposition and Eqs. 2 and 4 for nucleation and growth) for each case, and allow each system to evolve until the fraction of β phase reaches 95% of its equilibrium value; the time at which this value is attained is recorded as t_{eq}.

The values used for the various parameters in each model are presented in Table I. The mesh size, dx, and time step, dt, are also listed. The time step is chosen to be less than the maximum stable time step for either of Eqs. 2 and 4.

Upon the completion of each simulation, we use a modified Hoshen-Kopelmann algorithm to identify the clusters present in the system [1]. Because we are interested in the percolation threshold of the growing β phase, p_c^β, we identify clusters using level-set criteria $\psi > 0.5$

for nucleation and growth, and $c > 0.5$ for spinodal decomposition to determine whether a computational grid node is included in the α- or the β-phase. We then determine whether or not a spanning cluster is present, the average cluster size in the system, and the fraction of the system occupied by the largest cluster.

TABLE I: Model parameters for spinodal decomposition and nucleation and growth

	Spinodal Decomposition	Nucleation and Growth
dt	0.00001	0.001
dx	1/256	1/256
M_c	0.001	0.0001
M_ψ	N/A	1.0
F^{max}	1.0	N/A
c^α	0.119	N/A
c^β	0.881	N/A
ϵ_c	0.015	0.005
ϵ_ψ	N/A	0.005
$\tilde{W}_\psi$	N/A	10.0
$\tilde{L}$	N/A	20.0
$\tilde{T}_0$	N/A	0.4
τ	N/A	1.1
p_0^∞	N/A	0.1
r_0	N/A	2dx

III. SIMULATION RESULTS

Time lapse images of systems evolving through nucleation and growth and through spinodal decomposition at three equilibrium volume-fractions are presented in Fig. 1 and Fig. 2 respectively. Each type of microstructural evolution has a distinct visual characteristic that follows from its kinetics.

- Nucleation and growth (Fig. 1) results from a first order transition where the inserted nuclei are necessary to initiate the phase transformation. The nuclei initially grow by

absorbing solute that diffuses from the immediately surrounding media. Subsequently, some of the neighboring nuclei coalesce and form a network of the growth phase. At later stages, the microstructure evolves by a coarsening process wherein diffusion is driven by differences in surface curvature.

- Spinodal decomposition (Fig. 2) results from a second order transition where the system will evolve from an unstable initial uniform concentration whenever spatial perturbations exist. The decomposition proceeds as the amplitudes of fourier components of the initial perturbations grow until the concentrations approach c^α and c^β while maintaining the average system concentration. Only the amplitudes of those fourier components greater than some critical wavelength (λ_{crit}, see Eq. 12) will grow, and amplitudes for those components at a slightly larger wavelength, λ_{fast}, will grow the fastest. This additional length scale produces the characteristic (locally) lamellar microstructural features that become apparent in Fig. 2 at at $t_{eq}/4$. Visual inspection suggests that the systems resulting from spinodal decomposition form more connected networks of growth phase, suggesting that the percolation threshold should be lower for spinodal decomposition than nucleation and growth —this result is confirmed by the analysis presented below.

IV. PERCOLATION THRESHOLDS

The difference in percolation thresholds between the nucleation and growth and spinodal decomposition cases is apparent in Fig. 3 where the probability of percolation, Π, is plotted as a function of the equilibrium volume fraction of β-phase for systems at t_{eq}. We estimate Π at each p_∞ by computing the fraction of simulation runs containing a spanning cluster for each set of initial conditions. The decreasing width of the percolation transition as system size increases is also evident in these plots. By fitting each set of data with the empirical equation:

$$\Pi(p) = \frac{1}{2}\left[1 + \text{erf}\left(\frac{p - p_c^{\text{eff}}}{\Delta}\right)\right] \tag{5}$$

we obtain values for $p_c^{\text{eff}}(L)$ and $\Delta(L)$ at specific finite system sizes. An error function is used to fit the data because it converges to a step function in the limit $\Delta \to 0$. While the goodness of the fit for the larger system sizes in Fig. 3 may not be immediately apparent,

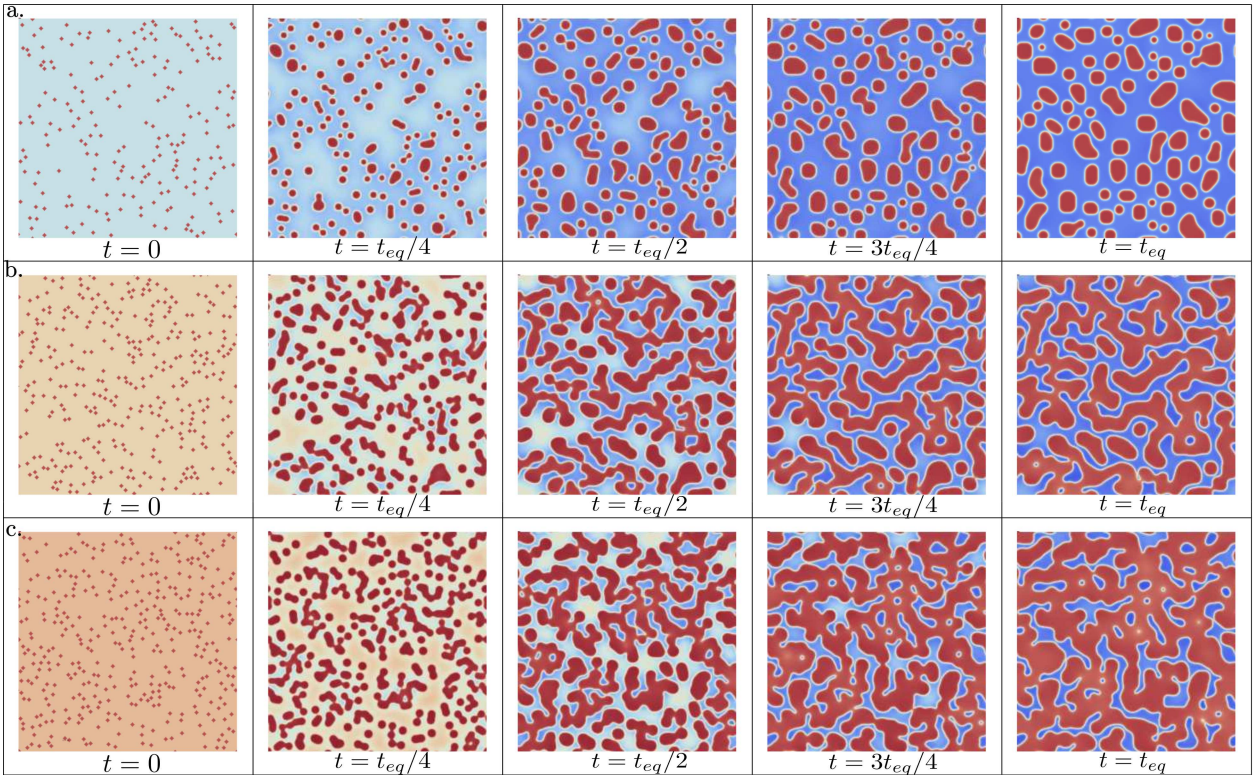

FIG. 1: (Color online) Sample time evolution of three systems generated by nucleation and growth with $p < p_c$ in (a), $p = p_c \approx 2/3$ in (b) and $p > p_c$ in (c). Images show the local concentration c_b with red (dark gray) corresponding to concentrations near c^β and blue (light gray) to concentrations near c^α. Bright regions occur at intermediate concentrations and highlight the phase boundaries.

viewing those systems alone on a smaller scale confirms that the fit is acceptable. We use the finite size scaling relations

$$p_c^{\text{eff}}(L) - p_c \propto L^{\frac{-1}{\nu}} \tag{6}$$

and

$$\Delta(L) \propto L^{\frac{-1}{\nu}} \tag{7}$$

to extrapolate the value of p_c as $\Delta \to 0$, $L \to \infty$, as shown in Fig. 4. This analysis yields $p_c = 0.499 \pm 0.003$ for spinodal decomposition, and $p_c = 0.661 \pm 0.003$ for nucleation and growth. For comparison, the percolation threshold for a randomly assigned square lattice is $p_c = 0.592746$ [1]. Continuum percolation of overlapping discs exhibits a threshold $p_c = 0.6764 \pm 0.0009$ when the discs have a uniform radius, and $p_c = 0.6860 \pm 0.0012$ for discs with a distribution of radii [3]. The overlapping disc values and the nucleation and growth value are similar, but differ by more than a standard deviation.

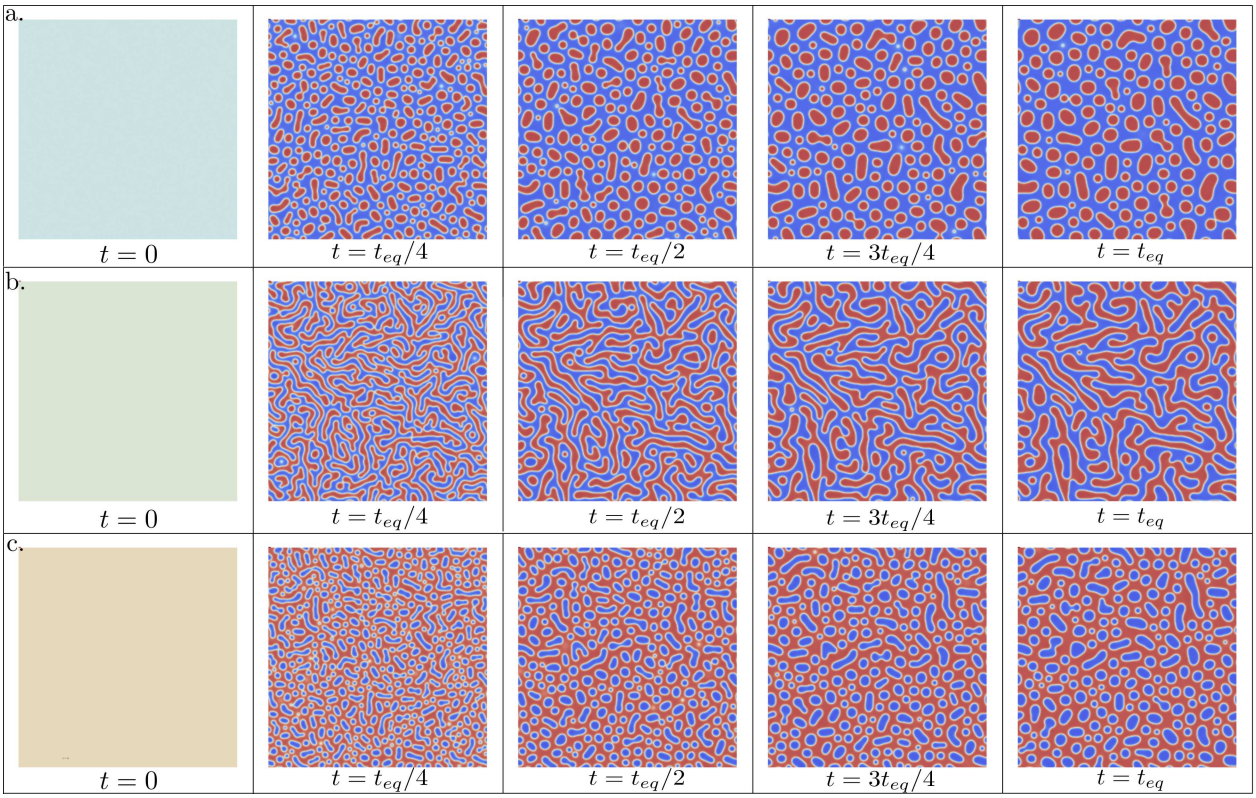

FIG. 2: (Color online) Sample time evolution of three systems generated by spinodal decomposition with $p < p_c$ in (a), $p = p_c \approx 1/2$ in (b) and $p > p_c$ in (c). Images show the local concentration c_b with red (dark gray) corresponding to concentrations near c^β and blue (light gray) to concentrations near c^α. Bright regions occur at intermediate concentrations and highlight the phase boundaries.

The observed percolation threshold for spinodal decomposition is explained by considering that the system is symmetric with respect to phase inversions. This fact, in combination with the fact that only one of the phases can form a percolating network in two dimensions requires that the percolation threshold be $p_c = 1/2$, and our data supports this conclusion. The three dimensional case is likely to be more interesting for spinodally decomposed systems as it is possible for a bicontinuous network to form, although phase inversion symmetry should remain. We speculate that the highly connected lamellar structure formed in a spinodally decomposed system would lead to a relatively low percolation threshold in three dimensions.

The observed percolation threshold ($p_c \approx 0.661$) for nucleation and growth is significantly higher than that of both spinodal decomposition and the random square lattice. We speculate this may be associated with the formation of a depletion region around the growing nuclei. At early stages of growth when the region surrounding a nucleus is oversaturated,

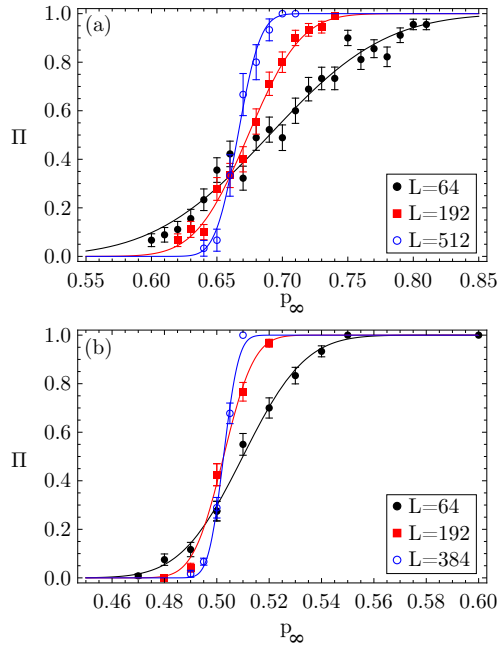

FIG. 3: (Color online) Probability of having a spanning cluster present plotted against equilibrium volume fraction of growth phase at various system sizes for nucleation and growth (a) and spinodal decomposition (b).

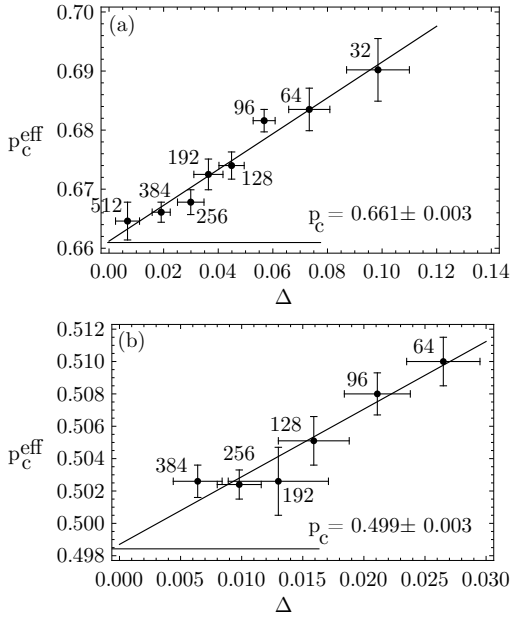

FIG. 4: Extrapolation of p_c based on the scaling of the effective percolation threshold with the width of the percolation transition for nucleation and growth (a) and spinodal decomposition (b).

two neighboring nuclei will coalesce if there is enough solute between them to form a connecting bridge. As the supersaturation decreases, the remaining neighboring distinct nuclei become separated by a region that is relatively depleted and they compete for solute. The effect would be similar to a hard core repulsion of the remaining nuclei. Thus, there is a transition from a process that is network-forming to one that is network-resistant.

A. Critical Exponents

The behavior of many quantities that diverge near the percolation threshold follow a simple power law of the form:

$$X \propto |p - p_c|^b \tag{8}$$

where X is the quantity of interest, and b is a critical exponent [4]. The universality hypothesis states that the values of the critical exponents depend solely on the dimensionality of the system, and not on its structure [3, 20, 21, 36]. We examined the critical behavior of our diffusionally evolved systems to verify conformity to the expected scaling. We focused on three critical exponents, ν, β, and γ. As seen earlier, ν is related to finite size scaling. To determine the value of ν we examine the relationship between p_c^{eff} and $\Delta(L)$. The exponent β is related to the scaling of the fraction of sites in the largest cluster, P, around p_c [1]. γ describes the scaling of the mean cluster mass, S, around p_c, with S defined as:

$$S = \frac{\Sigma_s s^2 n_s}{\Sigma_s n_s}$$

where n_s is the number of clusters containing s lattice sites [1].

The value of the critical exponent ν is estimated based on the scaling behavior of $p_c^{\text{eff}} - p_c$ with system size as described in Equation (6), and is shown in Fig. 5, in double logarithmic fashion. From these data, we obtain an estimate $\nu = 1.3 \pm 0.5$ for spinodal decomposition, and $\nu = 1.4 \pm 0.4$ for nucleation and growth. For both processes, the fits are not distinguishable from the dashed lines in Fig. 5 that correspond to the exact value $\nu = 4/3$. The amplitudes of the power law fit for ν (as well as those for β and γ) using the universal exponent values are tabulated in Table II.

β is estimated from the scaling behavior of the strength of the spanning cluster at the percolation threshold, $P(p_c, L)$. This quantity has been shown to scale according to:

$$P(p_c, L) \propto L^{-\frac{\beta}{\nu}} \tag{9}$$

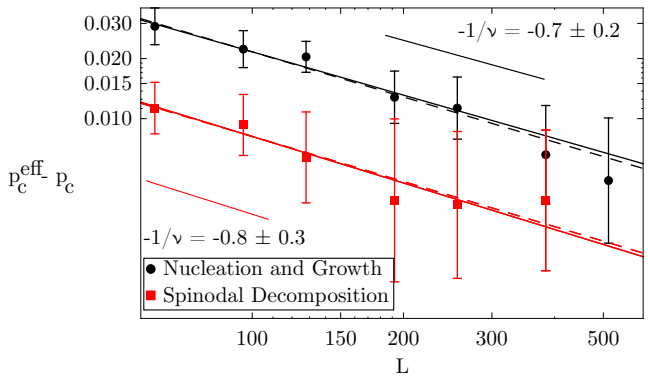

FIG. 5: (Color online) Extrapolation of ν based on a $\log_{10}$-$\log_{10}$ plot showing the finite size scaling of the effective percolation threshold. Solid lines are a least squares fit to the data, dashed lines are a least squares fit with the critical exponent set to the known value, 4/3, for two dimensional random percolation.

for systems of finite size L at $p = p_c$ [4]. β is estimated from the slope of the data in Fig. 6, which yields $\frac{\beta}{\nu} = 0.22 \pm 0.06$ for spinodal decomposition and $\frac{\beta}{\nu} = 0.19 \pm 0.03$ for nucleation and growth. Using the universal value $\nu = 4/3$ gives $\beta = 0.29 \pm 0.08$ for spinodal decomposition, and $\beta = 0.26 \pm 0.04$ for nucleation and growth. The expected value for two dimensional systems is $\beta = \frac{5}{36} \approx 0.13889$ [1]. While the observed values of β differ slightly from the exact value for random two-dimensional percolation, the dashed lines in Fig. 6 showing the fit using the universal exponents fall well within the error bars. The data plotted in Fig. 6 as well as Fig. 7 is from 60-250 simulations performed at each system size (fewer simulations were run for the larger systems because of limited computational resources) and the error bars are ± 1 standard deviation properly scaled to the logarithmic axes.

The scaling parameter γ speaks to the mean cluster mass $S(p_c, L)$ and its scaling behavior is given by:

$$S(p_c, L) \propto L^{\frac{\gamma}{\nu}} \tag{10}$$

for systems at $p = p_c$ [4]. Therefore the slope of the double logarithmic plot in Fig. 7 gives $\frac{\gamma}{\nu} = 2.10 \pm 0.09$ for spinodal decomposition, and $\frac{\gamma}{\nu} = 2.37 \pm 0.05$ for nucleation and growth. Using the universal value $\nu = 4/3$ in each case to solve for γ gives $\gamma = 2.8 \pm 0.1$ for spinodal decomposition and $\gamma = 3.16 \pm 0.07$ for nucleation and growth. The expected value for a two dimensional system is $\gamma = \frac{43}{18} \approx 2.3889$. As in the case for the estimates of β, the estimates

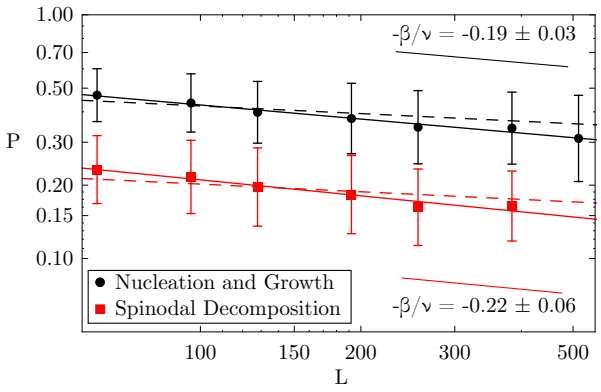

FIG. 6: (Color online) Extrapolation of β based on a $\log_{10}$-$\log_{10}$ plot showing the finite size scaling of the fraction of sites belonging to the spanning cluster. Solid lines are a least squares fit to the data, dashed lines are a least squares fit with the critical exponent set to the known value for two dimensional random percolation, 5/36.

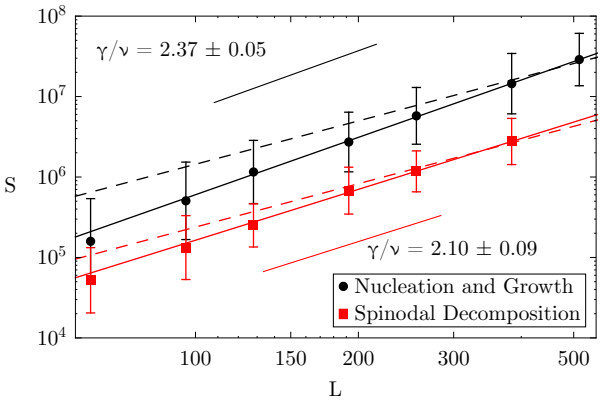

FIG. 7: (Color online) Extrapolation of γ based on a $\log_{10}$-$\log_{10}$ plot showing the finite size scaling of the average cluster mass. Solid lines are a least squares fit to the data, dashed lines are a least squares fit with the critical exponent set to the known value for two dimensional random percolation, 43/18.

of γ for both cases differ from the expected value; again, the dashed lines in Fig. 7 show that the difference is not large.

V. MICROSTRUCTURAL CORRELATION ANALYSIS

To relate the observed shifts in percolation threshold to the microstructural effects of the phase transformation types, we characterize their spatial correlations. We use the pair

TABLE II: Power law fit amplitudes using universal exponents

	Nucleation and Growth	Spinodal Decomposition
Fig. 5: $p_c^{\text{eff}}(L) - p_c$	$0.683\ L^{\frac{-1}{\nu}}$	$0.258\ L^{\frac{-1}{\nu}}$
Fig. 6: $P(p_c, L)$	$0.660\ L^{\frac{\beta}{\nu}}$	$0.326\ L^{\frac{\beta}{\nu}}$
Fig. 7: $S(p_c, L)$	$375.7\ L^{\frac{\gamma}{\nu}}$	$62.3\ L^{\frac{\gamma}{\nu}}$

correlation function, $g_{ij}(r)$ defined by:

$$g_{ij}(r) = \frac{\langle N_j(r) \rangle_i}{N(r)} \frac{1}{c_j} \tag{11}$$

where i and j are indices corresponding to the α- and β-phases present in the system, $\langle N_j(r) \rangle_i$ is the ensemble average number of sites at distance r from a site of phase i that contain phase j, $N(r)$ is the total number of sites at distance r, and c_j is the phase fraction of phase j. Therefore regions where $g_{ij}(r) = 1$ correspond to no correlation, regions where $g_{ij}(r) > 1$ correspond to the presence of more phase j than expected based on its phase fraction, and regions where $g_{ij}(r) < 1$ correspond to the presence of less phase j than expected. Because our systems are on a square computational grid and are isotropic on average, we only considered distances $r = n\text{dx}$ corresponding to sites that are separated by an integral number of grid spacings in the x-direction. This "horizontal counting" avoids the ambiguity of treating nodes near the edge of cylindrical shells on a square computational grid and fixes $N(r) = 2$.

Pair correlation functions for α-α, β-β and α-β interactions are plotted in Fig. 8. The functions are computed from fully evolved systems (t_∞) at the percolation threshold. For both spinodal decomposition and nucleation and growth, the correlations are short range. That is, $g(r)$ decays to 1 at long distances for all phase pairings. This confirms that the universal scaling relations of percolation theory should be applicable to systems formed through phase transformations. Furthermore, both types of systems have a short range region where $g_{ii}(r) > 1$, corresponding to phases tending to segregate from one another. Focusing on larger values of r we see that both types of systems exhibit some ordering since there is a region where $g_{ii}(r) < 1$. For spinodal systems this region appears because of the tendency of the system to form locally alternating stripes of the two phases due to the continuous nature of the phase transformation. This tendency also results in a third, smaller peak where $g(r) > 1$ that is not present for nucleation and growth, showing that

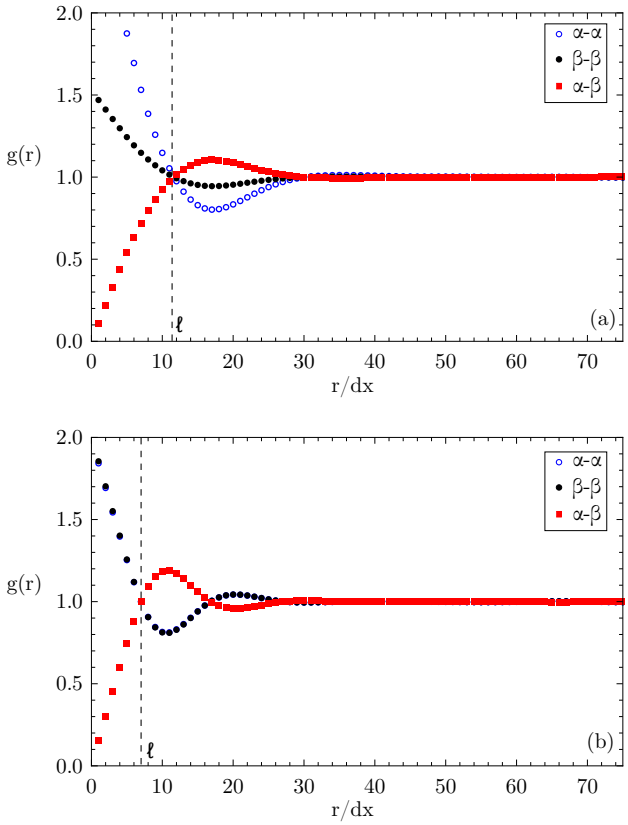

FIG. 8: (Color online) Pair correlation functions calculated from fully evolved (t_∞) systems generated by nucleation and growth (a) and spinodal decomposition (b). Both types of systems exhibit short range order. The width of the first correlation peak, ℓ, is marked by the dashed line.

spinodal systems exhibit somewhat longer range order. The first ordering peak observed for nucleated systems is likely a result of the formation of the depletion region (as described above) around a growing nucleus, causing the region immediately outside the nucleus to be more likely to consist of the α- (matrix) phase. There is no longer range order because the nuclei are initially placed randomly.

In order to relate the microstructural correlations for the two types of evolution, we compare the time-evolution of a characteristic length scale, $\ell(t)$, defined as the first crossing of $g_{\beta\beta}(r) = 1$ (cf. $\ell(t_\infty)$ in Fig. 8). We believe that this corresponds to the average particle size for nucleation and growth, and to half the wavelength of the fluctuations present in spinodally decomposed systems. Figure 9 depicts the growth in ℓ as a function of time on a ln-ln scale.

For nucleation and growth, there appear to be three regimes of evolution for the average

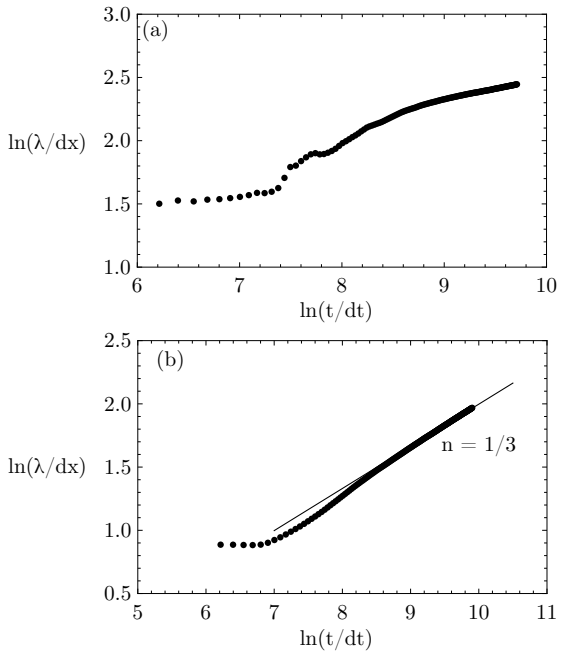

FIG. 9: Time evolution of the width of the first correlation peak, ℓ, for nucleation and growth (a) and spinodal decomposition (b). Regions where the data may be fit by a power law of the form $\ell \propto t^n$ are labeled.

particle size. We speculate that the regimes may be distinguished by the following processes: (i) at early times, all particles grow independently with short-range diffusion in a super-saturated matrix; (ii), at intermediate times, a small fraction of neighboring particles coalesce; (iii) at long times, a self similar coarsening process occurs in a depleted matrix. However, none of these regions fit well to a power law function with exponents predicted by mean field calculations of interface-limited or diffusion-limited processes (e.g., [45]). The first calculated value of $\ell(t = 500dt)$ is 4.49dx, which corresponds with the initial diameter of the nuclei in the system, $d = 4$dx, plus some growth in the first 500 time steps.

The evolution of $\ell(t)$ for spinodal systems is simpler. There is an initial region where ℓ is roughly constant. During this time the single phase lamella are developing from the initial concentration perturbations by transport of the B component between neighboring rich and dilute regions. We expect this initial length scale to correspond to the critical wavelength for spinodal decomposition, λ_{crit}:

$$\lambda_{\text{crit}} = \frac{\pi}{2}(c^{\beta} - c^{\alpha})\sqrt{\frac{\epsilon_c^2}{F^{max}}} \tag{12}$$

and the fastest growing wavelength is $\lambda_{\text{fast}} = \sqrt{2}\lambda_{\text{crit}}$ [45]. Using the parameter values

from the simulations $\lambda_{\text{crit}} = 4.60\text{dx}$ and $\lambda_{\text{fast}} = 6.50\text{dx}$. The first calculated value of ℓ at $t = 500\text{dt}$ is 2.43 which falls between $\lambda_{\text{crit}}/2$ and $\lambda_{\text{fast}}/2$. Once the single phase regions have reached their equilibrium concentrations the microstructure begins to coarsen and ℓ increases with time. At long times the coarsening fits well to a power law with exponent $n = 1/3$, corresponding to diffusion limited, curvature driven coarsening [48].

VI. CONCLUSIONS

In this paper we connect classical percolation concepts with the domain of structure evolution, two areas of the statistical physics literature that have traditionally been separate. Since phase correlations resulting from microstructural evolution processes lead to shifts in the percolation threshold in comparison to other methods of producing multi-phase systems, we believe that combining the knowledge of these two domains will allow scaling relations to be used for material property prediction in a broad range of practically relevant systems.

Examining the microstructures that evolve through nucleation and growth reveals two competing effects that alter the percolation threshold. We speculate that the increased p_c relative to the random square lattice involves the coalescence of neighboring nuclei at early stages of growth. Subsequent competition for solute in a depleted matrix during growth and curvature-driven coarsening impedes the coalescence of clusters, providing an explanation for the decreased p_c compared to randomly placed discs. For spinodal microstructures the primary source of phase correlations is the critical wavelength of stable perturbations that determines the initial microstructure. The quantitative analysis of the phase correlations present shows that only short range order is present in the phase distribution of microstructures derived from phase-transformations.

In addition to determining the value of the percolation threshold for these two types of microstructures, we also examined their critical behavior at p_c to confirm that the exponents ν, β, and γ are close to those observed in other two dimensional systems. Although our estimates have large statistical deviations (the number of computational experiments were resource limited), our estimates agree reasonably with the univerally observed exponents for other two dimensional systems. On the highest level the nature of the phase transformation does only one thing in regards to percolation: it introduces a state of correlations. These correlations affect the percolation scaling only if they are of infinite extent. Since phase

transformation induced correlations are all by definition local (diffusional fields, etc.), it is reasonable that the critical exponents are unchanged. It is important to note that this holds only for the percolation exponents, and not to confuse or conflate those with the time exponents of the transformation.

Acknowledgments

CAS acknowledges the support of the US National Science Foundation under contract DMR-0855402.

---

[1] D. Stauffer and A. Aharony, *Introduction to Percolation Theory*, vol. 2 (Taylor & Francis, 1992).

[2] S. Torquato, *Random Heterogeneous Materials* (Springer-Verlag, 2001).

[3] B. Lorenz, I. Orgzall, and H. O. Heuer, Journal of Physics A: Mathematical and General **26**, 4711 (1993).

[4] M. D. Rintoul and S. Torquato, Journal of Physics A: Mathematical and General **30**, 585 (1997).

[5] D. Stauffer, Physics Reports **54**, 1 (1979).

[6] M. K. Phani and D. Dhar, Journal of Physics A: Mathematical and General **17**, (1984).

[7] S. W. Haan and R. Zwanzig, Journal of Physics A Mathematical and General **10**, 1547 (1977).

[8] W. T. Elam, A. R. Kerstein, and J. J. Rehr, Physical Review Letters **52**, 1516 (1984).

[9] G. E. Pike and C. H. Seager, Physical Review B **10**, 1421 (1974).

[10] C. H. Seager and G. E. Pike, Physical Review B **10**, 1435 (1974).

[11] K. M. Golden, S. F. Ackley, and V. I. Lytle, Science **282**, 2238 (1998).

[12] K. M. Golden, Annals of Glaciology **33**, 28 (2001).

[13] K. M. Golden, Physica B Condensed Matter **338**, 274 (2003).

[14] Y. P. Mamunya, Y. V. Muzychenko, P. Pissis, E. V. Lebedev, and M. I. Shut, Polymer Engineering & Science **42**, 90 (2002).

[15] J. N. Coleman, S. Curran, A. B. Dalton, A. P. Davey, B. McCarthy, W. Blau, and R. C. Barklie, Physical Review B **58**, R7492 (1998).

[16] R. Murphy, V. Nicolosi, and Y. Hernandez, Scripta Materialia **54**, 417 (2006).

[17] J. C. Grunlan, A. R. Mehrabi, M. V. Bannon, and J. L. Bahr, Advanced Materials **16**, 150 (2004), ISSN 1521-4095.

[18] Y. Bréchet, J. Y. Cavaillé, E. Chabert, L. Chazeau, R. Dendievel, L. Flandin, and C. Gauthier, Advanced Engineering Materials **3**, 571 (2001), ISSN 1527-2648.

[19] P. R. A. Campos, L. F. C. Pessoa, and F. G. Brady Moreira, Physical Review B **56**, 40 (1997).

[20] C. M. Chaves and B. Koiller, Physica A: Statistical and Theoretical Physics **218**, 271 (1995), ISSN 0378-4371.

[21] M. C. Medeiros and C. M. Chaves, Physica A: Statistical and Theoretical Physics **234**, 604 (1997), ISSN 0378-4371.

[22] S. Prakash, S. Havlin, M. Schwartz, and H. E. Stanley, Physical Review A **46**, R1724 (1992).

[23] R. F. Voss, R. B. Laibowitz, and E. I. Alessandrini, Physical Review Letters **49**, 1441 (1982).

[24] M. E. Frary and C. A. Schuh, Physical Review E **76**, 041108 (2007).

[25] A. Sadiq and M. A. Khan, Zeitschrift für Physik B Condensed Matter **39**, 131 (1980).

[26] L. Flandin, T. Prasse, R. Schueler, K. Schulte, W. Bauhofer, and J. Y. Cavaille, Physical Review B **59**, 14349 (1999).

[27] F. Carmona and J. Ravier, Physica B: Condensed Matter **338**, 247 (2003), ISSN 0921-4526.

[28] P. Grassberger, Journal of Physics A Mathematical and General **22**, 3673 (1989).

[29] M. A. Knackstedt, M. Sahimi, and A. P. Sheppard, Phys. Rev. E **61**, 4920 (2000).

[30] M. A. Knackstedt, M. Sahimi, and A. P. Sheppard, Phys. Rev. E **65**, 035101 (2002).

[31] U. Bauerschäfer and M. Schulz, Phys. Rev. E **54**, 1442 (1996).

[32] A. Coniglio, H. E. Stanley, and W. Klein, Phys. Rev. Lett. **42**, 518 (1979).

[33] A. Weinrib, Phys. Rev. B **29**, 387 (1984).

[34] D. E. Sanders and J. W. Evans, Phys. Rev. A **38**, 4186 (1988).

[35] A. Kapitulnik and G. Deutscher, Phys. Rev. Lett. **49**, 1444 (1982).

[36] S. B. Lee and S. Torquato, Phys. Rev. A **41**, 5338 (1990).

[37] A. Khanikaev, A. Granovskii, and J. Clerc, Physics of the Solid State **44**, 1611 (2002).

[38] D. W. Heermann and D. Stauffer, Zeitschrift für Physik B Condensed Matter **44**, 339 (1981).

[39] K. Nozaki and T. Itami, Journal of Physics: Condensed Matter **16**, 7763 (2004).

[40] L. Kornyei and F. Igloi, Physical Review E (Statistical, Nonlinear, and Soft Matter Physics) **75**, 011131 (pages 6) (2007).

[41] J. N. Roberts and L. M. Schwartz, Phys. Rev. B **31**, 5990 (1985).

[42] C. Unger and W. Klein, Physical Review B **29**, 2698 (1984),

[43] A. Sicilia, Y. Sarrazin, J. J. Arenzon, A. J. Bray, and L. F. Cugliandolo, Physical Review E **80**, 031121 (2009),

[44] J. Arenzon, A. Bray, L. Cugliandolo, and A. Sicilia, Eur. Phys. J. B **64**, 403 (2008),

[45] R. W. Balluffi, S. M. Allen, and W. C. Carter, *Kinetics of Materials* (John Wiley & Sons, Inc., 2005).

[46] A. A. Wheeler, G. B. McFadden, and W. J. Boettinger, Proceedings: Mathematical, Physical and Engineering Sciences **452**, 495 (1996).

[47] W. J. Boettinger, J. A. Warren, C. Beckermann, and A. Karma, Annual Review of Materials Research **32**, 163 (2002).

[48] A. J. Bray, Philosophical Transactions of the Royal Society A: Mathematical, Physical and Engineering Sciences **361**, 781 (2003), ISSN 1364-503X.

[49] The ∞ subscript is used to indicated the phase fraction that applies as the simulation time approaches ∞ for infinite size systems. We consider a symmetric phase diagram in this paper: $1/2 - c^{\alpha} = c^{\beta} - 1/2$. We do not consider whether the functional form of double-well potential affects the p_c that we compute below

[50] Each nucleus has a size that will grow, i.e., none are sub-critical for the initial concentration field.